



**HAL**  
open science

# Modeling 1-D elastic P-waves in a fractured rock with hyperbolic jump conditions

Bruno Lombard, Joël Piriaux

► **To cite this version:**

Bruno Lombard, Joël Piriaux. Modeling 1-D elastic P-waves in a fractured rock with hyperbolic jump conditions. 2005. hal-00009406v1

**HAL Id: hal-00009406**

**<https://hal.science/hal-00009406v1>**

Preprint submitted on 3 Oct 2005 (v1), last revised 14 Mar 2006 (v3)

**HAL** is a multi-disciplinary open access archive for the deposit and dissemination of scientific research documents, whether they are published or not. The documents may come from teaching and research institutions in France or abroad, or from public or private research centers.

L'archive ouverte pluridisciplinaire **HAL**, est destinée au dépôt et à la diffusion de documents scientifiques de niveau recherche, publiés ou non, émanant des établissements d'enseignement et de recherche français ou étrangers, des laboratoires publics ou privés.

# Modeling 1-D elastic P-waves in a fractured rock with hyperbolic jump conditions

Bruno Lombard, Joël Piraux

*Laboratoire de Mécanique et d'Acoustique,  
31 chemin Joseph Aiguier, 13402 Marseille, France*

---

## Abstract

The one-dimensional propagation of compressional elastic waves in a fractured rock is investigated in the time-domain. The interaction between elastic waves and fractures are modeled by hyperbolic jump conditions deduced from a nonlinear contact law used in geomechanics. Existence and uniqueness of the solution to elastodynamics with the hyperbolic jump condition is proven. Numerical modeling is performed by coupling a finite-difference scheme with an interface method to account for the jump conditions. The numerical experiments proposed show the effects of contact nonlinearities, such as the generation of harmonics.

*Key words:* elastic waves, contact nonlinearity, Bandis-Barton model, jump conditions, finite-difference schemes, interface method.

*PACS:* 02.60.Cb, 02.70.Bf, 43.25.+y, 46.50.+a

---

## 1 Introduction

Fractures are the breaks in rocks caused by the huge stresses resulting from plate tectonics. It is of fundamental importance for geophysicists to be able to determine the position and the properties of fractures (such as their thickness) to be able to make predictions about the mechanical properties of a fractured platform or the diffusion of a pollutant, for instance. Elastic waves are commonly used for this purpose. When the wavelengths are much larger than the distance between fractures, the latter are generally not studied individually, and homogenization theories are applied. Otherwise, as in the case

---

*Email addresses:* lombard@lma.cnrs-mrs.fr (Bruno Lombard),  
piraux@lma.cnrs-mrs.fr (Joël Piraux).

*URL:* <http://w3lma.cnrs-mrs.fr/~MI/> (Bruno Lombard).

of the present study, it is possible to study single fractures. If, in addition, the wavelengths are much larger than the thickness of the fractures, the latter can be modeled in terms of interfaces with appropriate jump conditions.

Many experimental, theoretical and numerical studies have dealt with wave propagation across fractures in terms of the linear jump conditions [9,10,6]. The linear framework provides an appealing approach but it may not be very realistic, since non-physical penetration of both sides of the fractures may occur. Some authors have proposed more accurate fracture models, such as the Bandis-Barton model [1]. This model is frequently used in geomechanics to deal with quasi-static configurations. To our knowledge, [12] is the only author to have studied wave propagation in a model of this kind so far, with an analytical approach.

Here we present a numerical modeling approach to this configuration. Mathematical results are given in section 3: conservation of an energy, existence and uniqueness of the solution. Numerical methods are proposed in section 4; in particular, jump conditions are included in finite-difference schemes by adapting an interface method previously developed for dealing with linear contacts [8,6]. The numerical experiments performed in section 5 with realistic parameters show the influence of amplitudes of incident waves. Even with moderate amplitudes (the use of a linear elastodynamic framework outside the fracture is then fully justified), it may be necessary to take the nonlinear behavior of the fracture into account.

## 2 Problem statement

### 2.1 Configuration

Consider a rock with a single plane fracture. Outside the fracture, the media involved  $\Omega_i$  ( $i = 0, 1$ ) are linearly elastic and isotropic; they are subject to a constant static stress  $-\bar{\sigma}$  ( $\bar{\sigma} > 0$ ) running perpendicular to the fracture. At rest, the fractured zone is an *interphase* with thickness  $\bar{h} > 0$  (figure 1, left part). The nonlinear mechanical behavior of the interphase is investigated below (in section 2.2).

Let us take a plane compressional wave propagating through  $\Omega_0$  normally to the interphase; the interactions between this incident wave and the interphase give rise to reflected (in  $\Omega_0$ ) and transmitted (in  $\Omega_1$ ) plane compressional waves. These perturbations are described by the simple one-dimensional equations

$$\rho \frac{\partial v}{\partial t} = \frac{\partial \sigma}{\partial x}, \quad \frac{\partial \sigma}{\partial t} = \rho c^2 \frac{\partial v}{\partial x}, \quad (1)$$

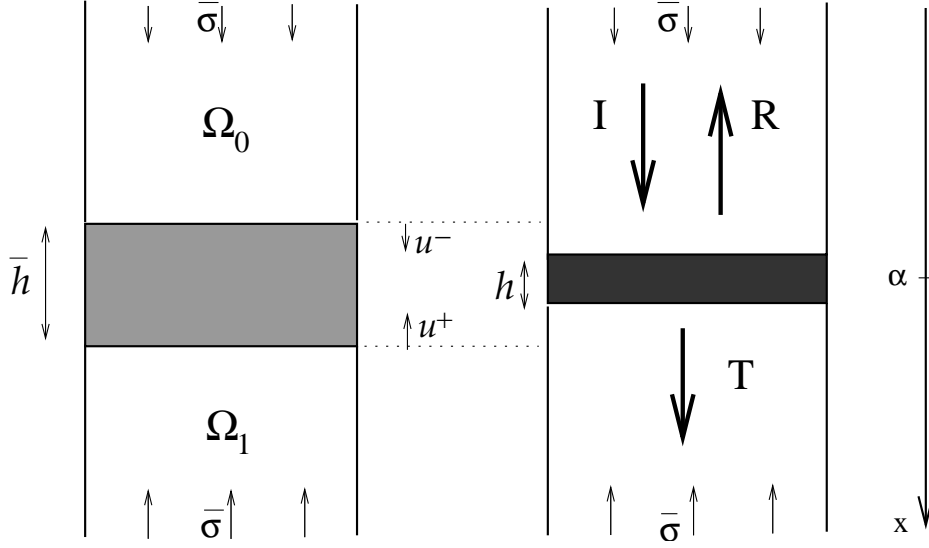


Fig. 1. Static (left) and dynamic (right) behavior of the fractured rock. I: incident wave; R: reflected wave; T: transmitted wave.

where  $v = \frac{\partial u}{\partial t}$  is the elastic velocity,  $u$  is the elastic displacement, and  $\sigma$  is the elastic stress perturbation around  $-\bar{\sigma}$ . The physical parameters involved are the density  $\rho$  and the elastic speed of the compressional waves  $c$ ; these parameters can be discontinuous and piecewise constant around the fracture:  $(\rho_0, c_0)$  if  $x \in \Omega_0$ ,  $(\rho_1, c_1)$  if  $x \in \Omega_1$ . The dynamic stresses induced by the elastic waves affect the thickness  $h(t)$  of the interphase (figure 1, right part). Due to the finite compressibility of the interphase, the constraint

$$h = \bar{h} + [u] \geq \bar{h} - d > 0 \quad (2)$$

must be satisfied, where  $[u] = u^+ - u^-$  is the difference between the elastic displacements on the two sides of the interphase, and  $d > 0$  is the *maximum allowable closure* [1]. We also assume that the wavelengths of the elastic perturbations are much larger than  $h$ . One can therefore neglect the propagation time through the interphase, and replace it by a zero-thickness *interface* at  $x = \alpha$ ; therefore,  $[u] = [u(\alpha, t)] = u(\alpha^+, t) - u(\alpha^-, t)$ . This is not in contradiction with what stated above, i.e., that (2) must be satisfied.

Setting up

$$\mathbf{U} = \begin{pmatrix} v \\ \sigma \end{pmatrix}, \quad \mathbf{A} = \begin{pmatrix} 0 & -\frac{1}{\rho} \\ -\rho c^2 & 0 \end{pmatrix}, \quad (3)$$

we deduce from what precedes the following initial-boundary value problem

$$\begin{cases} \frac{\partial}{\partial t} \mathbf{U} + \mathbf{A} \frac{\partial}{\partial x} \mathbf{U} = \mathbf{0} & \text{for } x \in \mathbb{R}, \quad x \neq \alpha, \quad t \geq t_0, \\ \mathbf{U}(x, t_0) = \mathbf{U}_0(x) & \text{for } x \in \mathbb{R}, \end{cases} \quad (4)$$

where  $U_0(x)$  is a  $C_c^p(\mathbb{R})$  function with a compact support included in  $\Omega_0$ . We assume that  $p \geq 1$ .

## 2.2 Jump conditions

Single fractures have been classically modeled in terms of linear jump conditions [9]. Given a *stiffness*  $K > 0$  and neglecting the inertial effects, the most usual linear conditions are

$$\begin{aligned} [\sigma(\alpha, t)] &= 0, \\ [u(\alpha, t)] &= \frac{1}{K} \sigma(\alpha^-, t). \end{aligned} \tag{5}$$

The simple jump conditions (5) can be rigorously obtained by performing an asymptotic analysis of the wave propagation process within a plane interphase which is much thinner than wavelength ( $h \ll \lambda$ ); then  $K = \rho c^2/h$ , where  $\rho$  and  $c$  are the physical parameters of the interphase. For  $K \rightarrow +\infty$ , we obtain perfectly-bonded conditions; for  $K \rightarrow 0^+$ , we obtain  $\sigma(\alpha^\pm, t) \rightarrow 0$ , and hence the two media  $\Omega_0$  and  $\Omega_1$  tend to be disconnected. The main drawback of these conditions (5) is that they do not satisfy (2): under large compressions loads,  $\sigma(\alpha^-, t) < -Kd \Rightarrow h < \bar{h} - d$ , which is in contradiction with (2). Hence, (5) are realistic only in the case of very small perturbations. When larger ones are involved, nonlinear jump conditions are required.

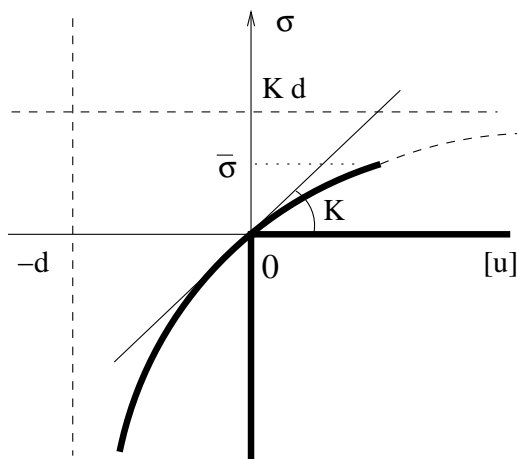


Fig. 2. Sketch of the stress-displacement relation in the Bandis-Barton model. The bold straight segments denote the limit-case of unilateral contact.

To satisfy (2), we use the Bandis-Barton model [1]. This model is based on quasi-static compressional experiments showing that the closure of a fracture depends hyperbolically on the stress applied. In the case of dynamic problems,

these hyperbolic jump conditions can be written [12]

$$\boxed{\begin{aligned} [\sigma(\alpha, t)] &= 0, \\ [u(\alpha, t)] &= \frac{1}{K} \frac{\sigma(\alpha^-, t)}{1 - \frac{\sigma(\alpha^-, t)}{Kd}}. \end{aligned}} \quad (6)$$

The second relation in (6) is sketched in figure 2; note that  $\sigma(\alpha^-, t) < Kd$  is always satisfied. Under compression loadings:  $\sigma(\alpha^\pm, t) < 0$ , the second equation of (6) implies:  $[u(\alpha, t)] > -d$ , so that (2) is always satisfied. Under traction loadings:  $\sigma(\alpha^\pm, t) > 0$ , the equations (6) are realistic up to  $\sigma(\alpha^\pm, t) = \bar{\sigma}$ ; above this level, the perturbations will disconnect the sides of the fracture. The straight line tangential to the hyperbola at the origin describes the linear jump conditions (5); as deduced from (6), the linear conditions are valid only if  $\sigma(\alpha^\pm, t) \ll Kd$ . Note the limit-case  $d \rightarrow 0^+$ : the hyperbola tends towards the nondifferentiable graph of unilateral contact, denoted by bold straight segments on figure 2. The latter corresponds to the Signorini's conditions [11]:  $\sigma(\alpha^+, t) = \sigma(\alpha^-, t) \leq 0$ ,  $[u(\alpha, t)] \geq 0$ , and  $\sigma(\alpha^+, t) [u(\alpha, t)] = 0$ . This limit-case, which leads to a difficult mathematical analysis and which requires adequate numerical tools, is not investigated here.

For use in section 4.2, we need the jump conditions to be satisfied by  $\mathbf{U}$  and its spatial derivatives, up to a given order. We assume the solution to be sufficiently smooth for the limit values of the spatial derivatives to be well-defined. First we differentiate the second equation of (6) with respect to  $t$ , and we replace the time derivative by a spatial derivative via (1)

$$\begin{aligned} \sigma(\alpha^+, t) &= \sigma(\alpha^-, t), \\ v(\alpha^+, t) &= v(\alpha^-, t) + \frac{1}{K} \frac{1}{\left(1 - \frac{\sigma(\alpha^-, t)}{Kd}\right)^2} \frac{\partial \sigma}{\partial t}(\alpha^-, t), \\ &= v(\alpha^-, t) + \frac{\rho_0 c_0^2}{K} \frac{1}{\left(1 - \frac{\sigma(\alpha^-, t)}{Kd}\right)^2} \frac{\partial v}{\partial x}(\alpha^-, t). \end{aligned} \quad (7)$$

The second equation of the zero-th order conditions (7) is nonlinear; it also involves a first-order derivative  $\frac{\partial v}{\partial x}$ . Similar differentiations applied  $(m-1)$  times to (7) yield nonlinear  $m$ -th order jump conditions, that can be written

$$\frac{\partial^m}{\partial x^m} \mathbf{U}(\alpha^+, t) = \mathbf{D}_m \left( \mathbf{U}, \dots, \frac{\partial^m}{\partial x^m} \mathbf{U}, \frac{\partial^{m+1}}{\partial x^{m+1}} \mathbf{U} \right) (\alpha^-, t), \quad (8)$$

where  $\mathbf{D}_m$  is a system of two nonlinear equations. This tedious task can easily be automated by using computed algebra tools.

### 3 Mathematical analysis

The aim of this section is to prove existence and uniqueness of the solution to elastodynamics (4) with the nonlinear jump conditions (6). Our proof is constructivist, leading to an analytical solution. The numerical evaluation of the latter constitutes the reference solution used in section 5. Before giving the theorem, we need some intermediate results. As a first lemma, we define an energy, and we show that it is conserved.

**Lemma 1** *Let  $\mathbf{U}(x, t)$  be a solution of (4)-(6). Then, the quantity*

$$E(\mathbf{U}, t) = \frac{1}{2} \int_{-\infty}^{+\infty} \left( \rho v^2 + \frac{1}{\rho c^2} \sigma^2 \right) dx + K d^2 \left( \ln \left( 1 - \frac{\sigma(\alpha^-, t)}{K d} \right) + \frac{1}{1 - \frac{\sigma(\alpha^-, t)}{K d}} - 1 \right) \quad (9)$$

*satisfies*

$$\frac{dE(\mathbf{U}, t)}{dt} = 0, \quad E(\mathbf{U}, t) \geq 0, \quad E(\mathbf{U}, t) = 0 \Leftrightarrow \mathbf{U}(x, t) = \mathbf{0}.$$

**PROOF.** We multiply the first equation of (1) by  $v$ , and we integrate it by parts on  $\Omega_0$ ; then the second equation of (1) gives

$$\begin{aligned} \int_{-\infty}^{\alpha^-} \rho v \frac{\partial v}{\partial t} dx &= \int_{-\infty}^{\alpha^-} v \frac{\partial \sigma}{\partial x} dx, \\ &= v(\alpha^-, t) \sigma(\alpha^-, t) - \int_{-\infty}^{\alpha^-} \sigma \frac{\partial v}{\partial x} dx, \\ &= v(\alpha^-, t) \sigma(\alpha^-, t) - \int_{-\infty}^{\alpha^-} \frac{1}{\rho c^2} \sigma \frac{\partial \sigma}{\partial t} dx. \end{aligned}$$

In the same way, we obtain

$$\int_{\alpha^+}^{+\infty} \rho v \frac{\partial v}{\partial t} dx = -v(\alpha^+, t) \sigma(\alpha^+, t) - \int_{\alpha^+}^{+\infty} \frac{1}{\rho c^2} \sigma \frac{\partial \sigma}{\partial t} dx.$$

Adding the two previous equations gives:  $\Delta_1 + \Delta_2 = 0$ , where

$$\begin{aligned} \Delta_1 &= \int_{-\infty}^{+\infty} \rho v \frac{\partial v}{\partial t} dx + \int_{-\infty}^{+\infty} \frac{1}{\rho c^2} \sigma \frac{\partial \sigma}{\partial t} dx \\ &= \frac{d}{dt} \underbrace{\frac{1}{2} \int_{-\infty}^{+\infty} \left( \rho v^2 + \frac{1}{\rho c^2} \sigma^2 \right) dx}_{E_1}, \end{aligned}$$

and, using (7),

$$\begin{aligned}
\Delta_2 &= \sigma(\alpha^-, t) [v(\alpha, t)], \\
&= \frac{1}{K} \frac{\sigma(\alpha^-, t)}{\left(1 - \frac{\sigma(\alpha^-, t)}{Kd}\right)^2} \frac{\partial \sigma}{\partial t}(\alpha^-, t), \\
&= \frac{d}{dt} K d^2 \underbrace{\left( \ln \left(1 - \frac{\sigma(\alpha^-, t)}{Kd}\right) + \frac{1}{1 - \frac{\sigma(\alpha^-, t)}{Kd}} - 1 \right)}_{E_2}.
\end{aligned}$$

The quantity  $E = E_1 + E_2$  therefore satisfies  $\frac{dE}{dt} = 0$ ;  $E_1$  is obviously a positive definite quadratic form. It only remains to study the sign of  $E_2$ . Setting  $\theta = 1 - \sigma(\alpha^-, t)/(Kd)$ , a standard study of  $g(\theta) = \ln \theta + 1/\theta - 1$  for  $\theta > 0$  shows that  $g(\theta) \geq 0$ , and that  $g(\theta) = 0 \Leftrightarrow \theta = 1$ , i.e.  $\sigma(\alpha^-, t) = 0$ . From (6) and (11), one sees that  $\sigma(\alpha^-, t) = 0 \Leftrightarrow \sigma(\alpha^+, t)$  and  $v(\alpha^\pm, t) = 0$ .  $\square$

The lemma 1 means that (9) is an energy, which is split into two terms:  $E_1$  is the classical mechanical energy associated with the propagation of elastic waves outside the fracture.  $E_2$  is the mechanical energy associated with the nonlinear deformation of the fracture; since the nonlinear spring has a mass equal to zero (6),  $E_2$  amounts to a potential energy. Note that in the limit case  $\sigma(\alpha^-, t) \ll Kd$ , one gets  $E_2 \rightarrow \frac{1}{2K} \sigma^2(\alpha^-, t)$ , which recovers the well-known potential energy of a linear spring.

To express  $\mathbf{U}(x, t)$  in terms of limit-values of the fields at  $\alpha$ , we use now the *Riemann invariants*  $J^{R,L}$  that are constant along the *characteristics*  $\gamma_{R,L}$  [4]; for linear PDES's with constant coefficients, their expressions are very simple

$$\begin{cases} \gamma_R : \frac{dx}{dt} = +c \Rightarrow \left. \frac{dJ^R}{dt} \right|_{\gamma_R} = 0, & \text{with } J^R(x, t) = \frac{1}{2} \left( v - \frac{1}{\rho c} \sigma \right) (x, t), \\ \gamma_L : \frac{dx}{dt} = -c \Rightarrow \left. \frac{dJ^L}{dt} \right|_{\gamma_L} = 0, & \text{with } J^L(x, t) = \frac{1}{2} \left( v + \frac{1}{\rho c} \sigma \right) (x, t). \end{cases} \quad (10)$$

After some calculations, (6) and (10) give

$$\begin{aligned}
\sigma(\alpha^\pm, t) &= -\rho_1 c_1 v(\alpha^+, t), \\
v(\alpha^-, t) &= -\frac{\rho_1 c_1}{\rho_0 c_0} v(\alpha^+, t) + 2 J_0^R(\alpha - c_0(t - t_0), t_0),
\end{aligned} \quad (11)$$

where the subscript  $i$  on  $J_i^{R,L}$  refers to  $\Omega_i$ . The following lemma combined with (11) shows that  $\mathbf{U}(x, t)$  can be expressed in terms of  $\mathbf{U}_0(x)$ , and of  $v(\alpha^+, s)$  (with  $t_0 < s < t$ ).

**Lemma 2** *The solution  $\mathbf{U}(x, t)$  of (4) is given by*

$$\begin{cases} \underline{x < \alpha} : \\ \mathbf{U}(x, t) = \begin{pmatrix} 1 & 1 \\ -\rho_0 c_0 & \rho_0 c_0 \end{pmatrix} \begin{pmatrix} J_0^R(x - c_0(t - t_0), t_0) \\ \Delta_A(x, t) \end{pmatrix}, \\ \text{with } \Delta_A(x, t) = \begin{cases} J_0^L(\alpha^-, t_A) & \text{if } t_A = t - \frac{1}{c_0}(\alpha - x) \geq 0, \\ 0 & \text{otherwise,} \end{cases} \end{cases}$$

$$\begin{cases} \underline{x > \alpha} : \\ \mathbf{U}(x, t) = \begin{pmatrix} 1 \\ -\rho_1 c_1 \end{pmatrix} \Delta_B(x, t), \\ \text{with } \Delta_B(x, t) = \begin{cases} v(\alpha^+, t_B) & \text{if } t_B = t - \frac{1}{c_1}(x - \alpha) \geq 0, \\ 0 & \text{otherwise.} \end{cases} \end{cases}$$

PROOF. For  $x < \alpha$ , we deduce from (10) that

$$\begin{cases} J_0^R(x, t) = J_0^R(x - c_0(t - t_0), t_0), \\ J_0^L(x, t) = J_0^L(\alpha^-, t_A), \end{cases}$$

which leads directly to the result. For  $x > \alpha$ , we deduce from (10) that

$$\begin{cases} J_1^R(x, t) = J_1^R(x + c_1(t - t_0), t_0) \\ J_1^L(x, t) = J_1^L(\alpha^+, t_B). \end{cases}$$

Using (11) completes the proof.  $\square$

Up to now, we have not used the hyperbolic jump condition satisfied by  $u$  (6) or by  $v$  (7). This condition implies that  $v(\alpha^+, t)$  satisfies a nonlinear ordinary differential equation, as stated by the following lemma.

**Lemma 3** *The limit value  $y = v(\alpha^+, t)$  satisfies the nonlinear ODE*

$$\left\{ \begin{array}{l} \frac{dy}{dt} = f(y, t), \quad y(t_0) = 0, \quad \text{with} \\ f(y, t) = \frac{K}{\rho_1 c_1} \left(1 + \frac{\rho_1 c_1}{K d} y\right)^2 \left(g(t) - \left(1 + \frac{\rho_1 c_1}{\rho_0 c_0}\right) y\right), \\ g(t) = 2 J_0^R(\alpha - c_0(t - t_0), t_0). \end{array} \right. \quad (12)$$

PROOF. The initial value  $y(t_0) = 0$  follows from the compact support of  $\mathbf{U}_0(x)$  (see section 2.1). From (7) and (11), we obtain

$$\begin{aligned} v(\alpha^+, t) - v(\alpha^-, t) &= \frac{1}{K} \frac{1}{\left(1 - \frac{1}{K d} \sigma(\alpha^+, t)\right)^2} \frac{\partial \sigma}{\partial t}(\alpha^+, t), \\ &= -\frac{\rho_1 c_1}{K} \frac{1}{\left(1 + \frac{\rho_1 c_1}{K d} v(\alpha^+, t)\right)^2} \frac{\partial v}{\partial t}(\alpha^+, t). \end{aligned}$$

Then,  $v(\alpha^-, t)$  is eliminated via (11), leading to (12).  $\square$

We have now all the tools to prove the following theorem.

**Theorem 1** *There exists a unique global solution to (4)-(6).*

PROOF. As shown by lemmas 2 and 3, the exact solution of (4)-(6) is expressed in a unique manner in terms of  $v(\alpha^+, t)$  solution of the ODE (12). Proving the existence and uniqueness of the solution to (4)-(6) amounts therefore to showing the existence and uniqueness of  $y(t)$  solution to (12), as proven now.

$J_0^R(x, t_0)$  is a  $C_c^p$  function ( $p \geq 1$ ) deduced from  $\mathbf{U}_0(x)$ . For  $t > t_0$ ,  $y \rightarrow f(y, t)$  in (12) is therefore  $C^1$ , hence it is a locally Lipschitz function. Moreover, the time dependence  $g(t)$  in (12) is  $C_c^p$ , hence  $t \rightarrow f(y, t)$  is continuous. Then, the Cauchy-Lipschitz theorem ensures that the solution  $y(t)$  is unique, if it exists.

To show the existence of a global solution, suppose that  $y(t)$  is not bounded as  $t \rightarrow t^*$ ; (11) implies that  $\sigma(\alpha^-, t) \rightarrow \pm\infty$ . Since  $\sigma(\alpha^-, t) < K d$  (see section 2.2), only the case  $\sigma(\alpha^-, t) \rightarrow -\infty$  needs to be addressed. In that case, (9) implies that  $E(\mathbf{U}, t) \rightarrow +\infty$ , which is impossible: lemma 1 and  $\mathbf{U}_0 \in C_c^p$  imply that  $E(\mathbf{U}, t) = E(\mathbf{U}_0, t_0) < +\infty$ . Hence  $y(t)$  is always bounded, and the local existence due to Cauchy-Lipschitz theorem is also global [3].  $\square$

## 4 Numerical methods

### 4.1 Numerical scheme

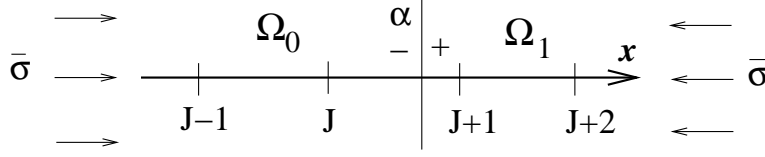


Fig. 3. 1D rock fractured at  $x = \alpha$ ; spatial mesh.

Given  $(x_i, t_n) = (i \Delta x, n \Delta t)$ , where  $\Delta x$  is the mesh size and  $\Delta t$  is the time step, we seek an approximation  $\mathbf{U}_i^n$  of  $\mathbf{U}(x_i, t_n)$ . We use two-step, explicit, and  $(2s+1)$ -point spatially-centered finite-difference schemes to integrate (4). Time-stepping is written symbolically via the discrete operator  $\mathbf{H}$

$$\mathbf{U}_i^{n+1} = \mathbf{U}_i^n + \mathbf{H}(\mathbf{U}_{i-s}^n, \dots, \mathbf{U}_{i+s}^n). \quad (13)$$

As observed in numerical experiments, sharp fronts can appear when the non-linear effects induced by the fracture are non negligible, even when starting with smooth initial data. It can therefore be worth using schemes which work well with shock waves. For this purpose, we use a second-order scheme with flux limiter [5] borrowed from computational fluid mechanics ( $s = 2$ , stable up to CFL = 1).

We define  $J$  so that  $x_J \leq \alpha < x_{J+1}$  (figure 3). A grid point is *regular* if its time-stepping does not cross the interface; in this case, (13) is applied classically. Otherwise, a grid point is *irregular*, and its time-stepping is described in the next section. The irregular points are  $x_{J-s+1}, \dots, x_{J+s}$ .

### 4.2 Interface method

To describe numerically the jump conditions (6), one applies the interface method [6,8]: at irregular points, some of the numerical values used for the time-stepping procedure (13) are modified; these *modified values* are computed and used as follows. At time  $t_n$  on each side of  $\alpha$ , we define a smooth extension  $\mathbf{U}^*(x, t_n)$  of  $\mathbf{U}(x, t_n)$  to the other side of  $\alpha$

$$\begin{aligned} x > \alpha, \quad \mathbf{U}^*(x, t_n) &= \sum_{m=0}^{2k-1} \frac{(x - \alpha)^m}{m!} \frac{\partial^m}{\partial x^m} \mathbf{U}(\alpha^-, t_n), \\ x \leq \alpha, \quad \mathbf{U}^*(x, t_n) &= \sum_{m=0}^{2k-1} \frac{(x - \alpha)^m}{m!} \frac{\partial^m}{\partial x^m} \mathbf{U}(\alpha^+, t_n). \end{aligned} \quad (14)$$

In practice we take  $k = 2$ , which is the optimum value for the scheme discussed in section 4.1 in the case of linear jump conditions (5), as established in [6]. To estimate the limit values in (14), we write Taylor expansions of  $\mathbf{U}(x_i, t_n)$  "on the left" of  $\alpha$  ( $i = J - k + 1, \dots, J$ )

$$\mathbf{U}(x_i, t_n) = \sum_{m=0}^{2k-1} \frac{(x_i - \alpha)^m}{m!} \frac{\partial^m}{\partial x^m} \mathbf{U}(\alpha^-, t_n) + \mathbf{O}(\Delta x^{2k}), \quad (15)$$

and "on the right" of  $\alpha$  ( $i = J + 1, \dots, J + k$ ), with the jump conditions (8)

$$\begin{aligned} \mathbf{U}(x_i, t_n) &= \sum_{m=0}^{2k-1} \frac{(x_i - \alpha)^m}{m!} \frac{\partial^m}{\partial x^m} \mathbf{U}(\alpha^+, t_n) + \mathbf{O}(\Delta x^{2k}) \\ &= \sum_{m=0}^{2k-1} \frac{(x_i - \alpha)^m}{m!} \mathbf{D}_m \left( \mathbf{U}, \dots, \frac{\partial^{m+1}}{\partial x^{m+1}} \mathbf{U} \right) (\alpha^-, t_n) + \mathbf{O}(\Delta x^{2k}). \end{aligned} \quad (16)$$

In (15) and (16), we replace  $\mathbf{U}(x_i, t_n)$  by  $\mathbf{U}_i^n$ , and we replace the exact limit values with their numerical estimates; Taylor remainders and  $\frac{\partial^{2k}}{\partial x^{2k}} \mathbf{U}(\alpha^-, t_n)$  are removed. This leads to the following nonlinear system

$$\mathbf{F} \left( \mathbf{U}(\alpha^-, t_n), \dots, \frac{\partial^{2k-1}}{\partial x^{2k-1}} \mathbf{U}(\alpha^-, t_n) \right) = \mathbf{0}, \quad (17)$$

which depends on  $\mathbf{U}_i^n$  ( $i = J - k + 1, \dots, J + k$ ). The  $4k \times 4k$  system (17) is solved using Newton's method, giving estimates  $\mathbf{U}_i^*$  for  $\mathbf{U}^*(x_i, t_n)$  (see (14)). The time-stepping at any irregular point  $x_i$  will therefore be

$$\begin{aligned} J - s + 1 \leq i \leq J, \quad \mathbf{U}_i^{n+1} &= \mathbf{U}_i^n + \mathbf{H} \left( \mathbf{U}_{i-s}^n, \dots, \mathbf{U}_J^n, \mathbf{U}_{J+1}^*, \dots, \mathbf{U}_{i+s}^* \right), \\ J + 1 \leq i \leq J + s, \quad \mathbf{U}_i^{n+1} &= \mathbf{U}_i^n + \mathbf{H} \left( \mathbf{U}_{i-s}^*, \dots, \mathbf{U}_J^*, \mathbf{U}_{J+1}^n, \dots, \mathbf{U}_{i+s}^n \right). \end{aligned} \quad (18)$$

In the limit case of a homogeneous medium without any fracture (i.e.,  $\rho_0 = \rho_1$ ,  $c_0 = c_1$ ,  $\sigma(\alpha^-, t) \ll Kd$ ,  $K \rightarrow +\infty$ ) and if  $k \geq s$ , then  $\mathbf{U}_i^* = \mathbf{U}_i^n$ : the interface method (18) amounts to the classical time-marching (13) (the proof of result 5 in [6] can be readily adapted). We have no theoretical results about the stability of the interface method; however, numerical experiments have shown that the CFL condition is not affected by  $K$  and  $d$ .

The nonlinear system (17) may have more than one solution, and nothing ensures that Newton's algorithm selects the good one. To investigate this point, we compare the "numerical" value  $v(\alpha^-, t_n)$  found by solving (17) with the "analytical" value obtained by numerically integrating the ODE (12) and using (11). In the case of weak to moderate nonlinear effects (empirically  $\sigma_0 < Kd/10$ , where  $\sigma_0$  is the amplitude of  $\sigma(x, t_0)$ ), the results are the same. But when the nonlinear effects are large, convergence towards a "wrong

solution” can occur if the mesh used is too coarse. This is not very surprising: since wave profiles tend to sharpen (see section 5), the Taylor expansions in (15) and (16) give rather poor estimates. The only strategy currently available here consists of refining the mesh.

## 5 Numerical experiments

We study a 400-m domain fractured at  $\alpha = 200.67$  m, which is described in terms of realistic parameters [12]

$$\begin{cases} \rho_0 = \rho_1 = 1200 \text{ kg/m}^3, & K = 1.3 \cdot 10^9 \text{ kg/s}^2, \\ c_0 = c_1 = 2800 \text{ m/s}, & d = 6.1 \cdot 10^{-4} \text{ m}. \end{cases}$$

Two incident waves are now considered, leading to the so-called ”Test 1” and ”Test 2”. In test 1, we take  $\mathbf{U}_0(x) = {}^T(-1/c_0, \rho_0) f(t - x / c_0)$  in (4), where  $f$  is a spatially-bounded  $C_c^2$  sinusoid

$$f(\xi) = \begin{cases} \varepsilon \left( \sin(\omega_c \xi) - \frac{1}{2} \sin(2\omega_c \xi) \right) & \text{if } 0 < \xi < \frac{1}{f_c}, \\ 0 & \text{else,} \end{cases} \quad (19)$$

$f_c = \omega_c / (2\pi) = 50$  Hz is the central frequency,  $t_0 = 52$  ms, and  $\varepsilon$  is an amplitude factor. This particular choice ensures that the incident wave is a purely right-going wave. Three values of  $\varepsilon$  are investigated, leading to three values of the amplitude  $v_0$  of  $v(x, t_0)$ : 0.01 m/s (a), 0.2 m/s (b), and 0.6 m/s (c). The computations are performed on 400 grid points (for cases (a) and (b)) or 1200 grid points (for case (c)). The Courant number is CFL = 0.9.

Figure 4 shows the numerical and analytical values of  $\sigma$  (left row), and the numerical values of  $[u]$  deduced from (6) and (17) (right row) at  $t = 116.91$  ms. In the right row, the horizontal dotted line represents  $-d$ , which is the limit value that must not be reached (see (2)). In case (a),  $v_0$  is too small to mobilize the nonlinearity of the fracture: no differences could be detected with simulations performed with (5). Case (b) corresponds to realistic seismic waves recorded during on-site investigations: large nonlinear effects are present. Case (c) corresponds to blasting waves: very large nonlinear effects are present, sharpening the fronts and leading to ”corners”. The solution is computed on a larger number of grid points than in cases (a-b): otherwise, the nonlinear system (17) would not have converged to the exact solution (see section 4.2).

The aim of test 2 is to simulate an experimental time-harmonic study. A sinusoidal source term is inserted into the numerical scheme at  $x = 40$  m. Three

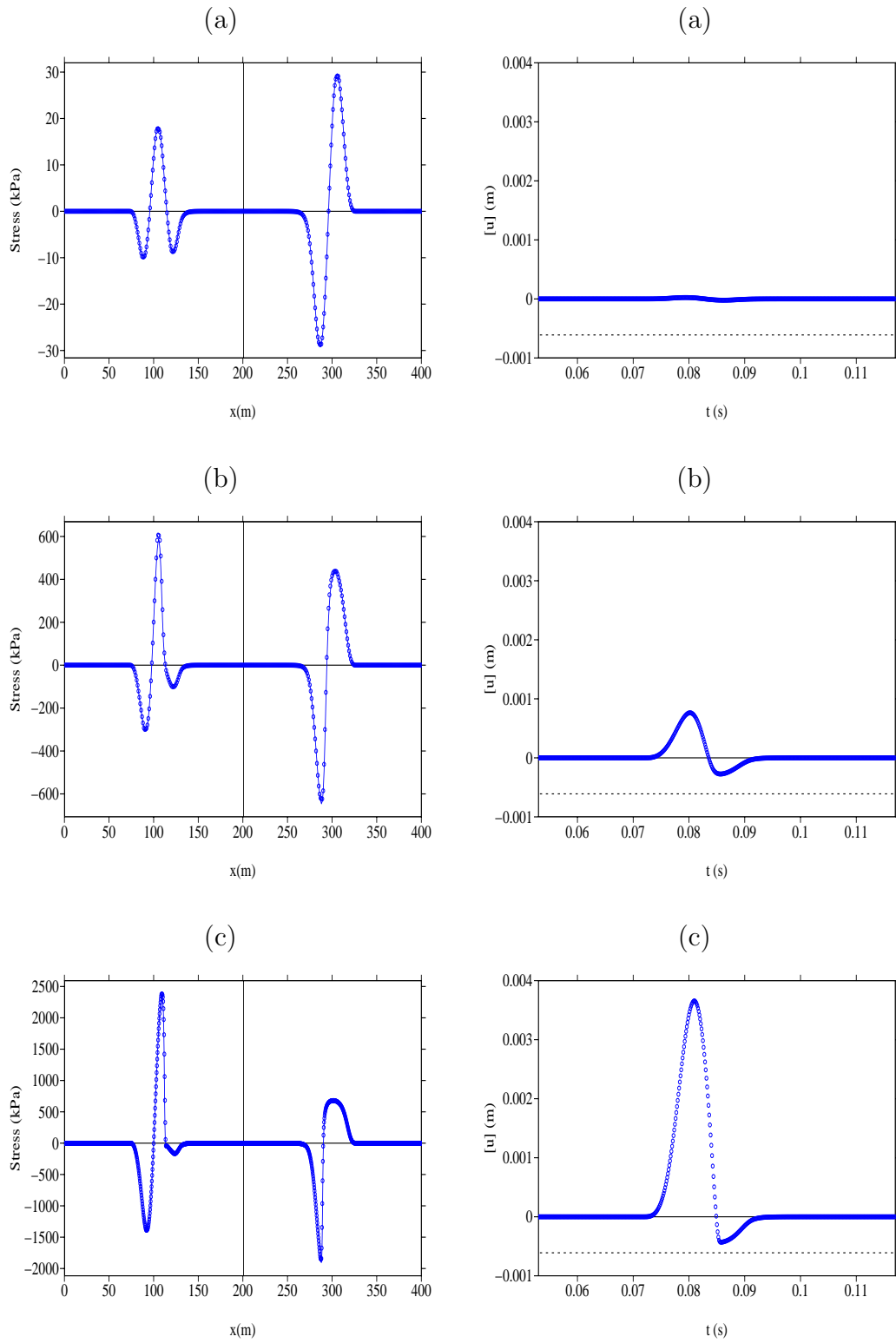


Fig. 4. Test 1:  $v_0 = 0.01$  m/s (a),  $v_0 = 0.2$  m/s (b), and  $v_0 = 0.6$  m/s (c). Left row: numerical (...) and "exact" (-) values of  $\sigma$ ; right row: numerical values of  $[u]$ .

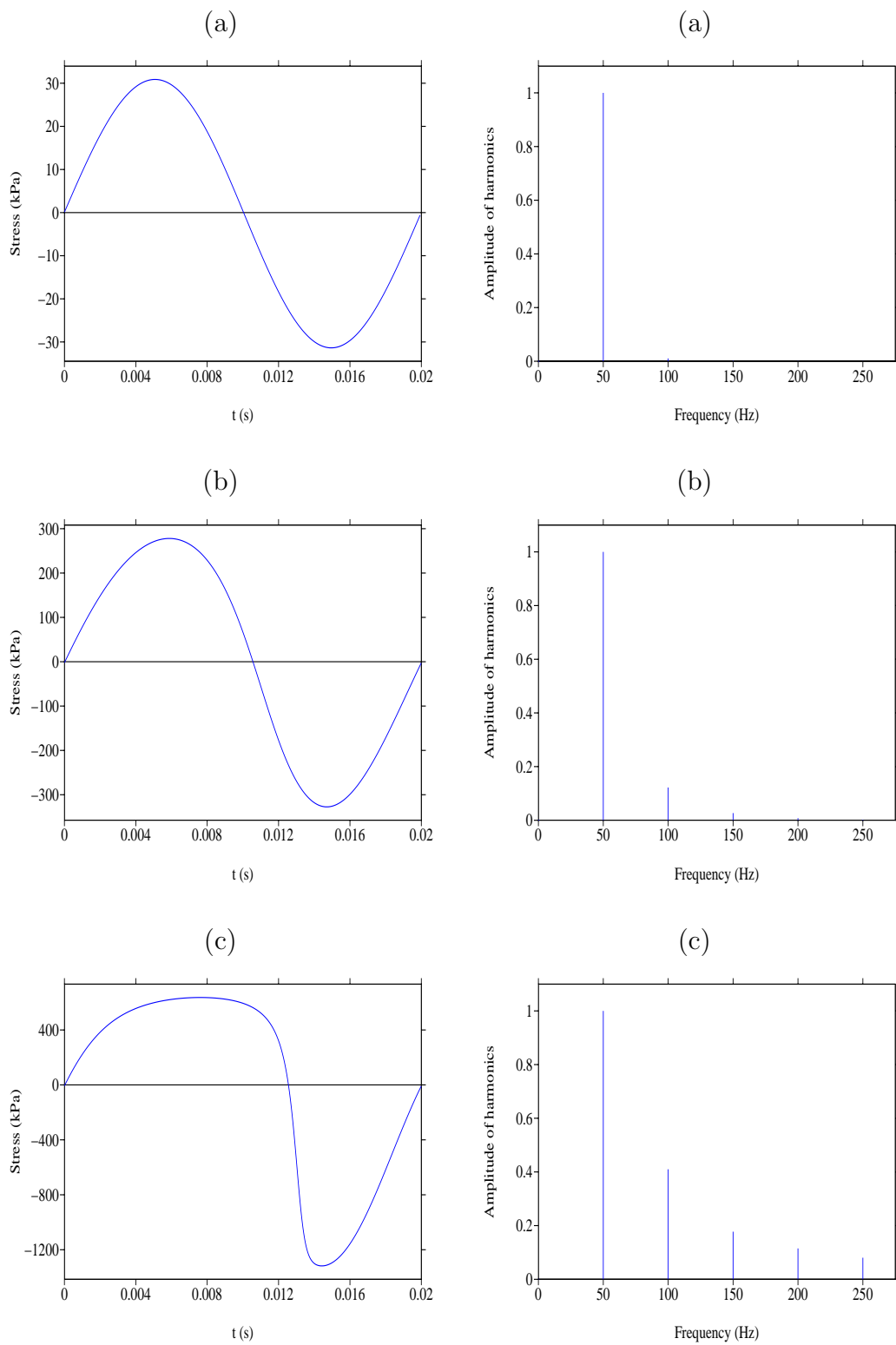


Fig. 5. Test 2:  $v_0 = 0.01$  m/s (a),  $v_0 = 0.1$  m/s (b), and  $v_0 = 0.4$  m/s (c). Left row: numerical values of  $\sigma$  during a period; right row: normalized coefficients of the Fourier decomposition.

source term amplitudes are used successively, yielding the three amplitudes  $v_0$ : 0.01 m/s (a), 0.1 m/s (b), and 0.4 m/s (c). The periodic values of the transmitted wave are recorded at  $x = 220$  m; a decomposition into Fourier series is then applied to these values. Figure 5 shows the numerical values of  $\sigma$  obtained during one period (left row), and the normalized coefficients of the Fourier series (right row). The harmonics generated when  $v_0$  increases can be clearly seen in this figure.

There are two main reasons for displaying these harmonics. First they help to decide whether it is worthwhile taking the nonlinear effects into account: solving the nonlinear system (17) at each time step is more costly from the computational point of view than solving a linear system during a pre-processing step, as established for the linear jump conditions (5) in [6]. In case (a), the answer is negative; in case (b), it depends on the accuracy required; in case (c), the answer is positive. Secondly, the stiffness  $K$  and the maximum allowable closure  $d$  can be inferred from the decrease in the harmonics. This makes it possible to inspect the state of the fracture.

## 6 Conclusion

Here we have studied the propagation of transient 1-D elastic compressional waves across a contact nonlinearity. The latter feature models a fracture in rocks, but it can also be a useful means of describing other physical situations, such as those encountered in the nondestructive evaluation of material for instance [2]. Our work involves a physical description of the model, a mathematical analysis of its solution, and a numerical time-domain modeling.

Many points still remain to be investigated. First, the regularity of the solution to (4)-(6) needs to be addressed: the presence of shocks or corners (which are observed numerically) has an influence on the choice of the numerical scheme. Secondly, the stability of the interface method is still an open question, even under linear jump conditions. Thirdly, it would be interesting to determine analytically the harmonics generated across the fracture, with the harmonic balance method (see test 2).

A similar study in 1D with elastic shear waves would have to take some additional interesting features into account, such as the friction laws and adhesion processes [1,7]. Interactions can occur between compressional and shear waves even in the 1-D context, because of the coupling between normal and tangential jump conditions. Our final goal is to develop a 2-D model.

**Acknowledgments.** We thank Denis Matignon (ENST Paris) for his careful reading and his advices.

## References

- [1] S. C. BANDIS, A. C. LUMSDEN, N. R. BARTON, *Fundamentals of rock fracture deformation*, Int. J. Rock Mech. Min. Sci. Geomech. Abstr., 20-6 (1983), pp. 249–268.
- [2] S. BIWA, S. NAKAJIMA, N. OHNO, *On the acoustic nonlinearity of solid-solid contact with pressure dependent interface stiffness*, ASME J. Appl. Mech., 71 (2004), pp. 508–515.
- [3] M. CROUZEIX, A. L. MIGNOT, *Analyse numérique des équations différentielles*, Masson, 1992.
- [4] E. GODLEWSKI, P. A. RAVIART, *Numerical Approximation of Hyperbolic Systems of Conservation Laws*, Springer-Verlag, 1996.
- [5] R. J. LEVEQUE, *Wave propagation algorithms for multi-dimensional hyperbolic systems*, J. Comput. Phys., 131 (1997), pp. 327–353.
- [6] B. LOMBARD, J. PIRAUX, *How to incorporate the spring-mass conditions in finite-difference schemes*, SIAM J. Scient. Comput., 24-4 (2003), pp. 1379–1407.
- [7] C. PECORARI, *Nonlinear interaction of plane ultrasonic waves with an interface between rough surfaces in contact*, J. Acoust. Soc. Am., 113-6 (2003), pp. 3065–3072.
- [8] J. PIRAUX, B. LOMBARD, *A new interface method for hyperbolic problems with discontinuous coefficients: 1D acoustic example*, J. Comput. Phys., 168-1 (2001), pp. 227–248.
- [9] L. PYRAK-NOLTE, L. MYER, N. COOK, *Transmission of seismic waves across single natural fractures*, J. Geophys. Res., 95-B6 (1990), pp. 8617–8638.
- [10] S. I. ROKHLIN, Y. J. WANG, *Analysis of boundary conditions for elastic wave interaction with an interface between two solids*, J. Acoust. Soc. Am., 89-2 (1991), pp. 503–515.
- [11] G. SCARELLA, *Etude théorique et numérique de la propagation d’ondes en présence de contact unilatéral dans un milieu fissuré*, PhD. thesis, Paris 9, 2004.
- [12] J. ZHAO, J. G. CAI, *Transmission of elastic P-waves across single fractures with a nonlinear normal deformational behavior*, Rock Mech. Rock Engng., 34-1 (2001), pp. 3–22.